

基于颅骨表面解剖标志的成人乙状窦后入路 关键孔定位

付涛 惠志强 宋杰 黄健 许鹏

【摘要】 目的 探讨通过乙状窦后入路手术中较易显露的颅骨表面解剖标志建立的坐标系在关键孔定位中的应用价值。**方法** 回顾分析 2019 年 1 月至 2020 年 1 月山东省临沂市中心医院影像科数据库内 80 例三叉神经痛或面肌痉挛患者计 160 侧颅骨薄层 CT 资料并三维成像,以二腹肌沟顶点(A点)、颞鳞与顶乳缝交点(B点)和星点(C点)构建影像学模型并探寻关键孔定位规律。再选择 2020 年 5 月至 2022 年 5 月在我院行乙状窦后入路微血管减压术的 60 例患者(三叉神经痛 33 例、面肌痉挛 25 例、舌咽神经痛 2 例),随机分为重建组、非重建组 and 对照组(各 20 例),重建组术中构建坐标系后,以术前影像学模型模拟的关键孔圆心定位关键孔;非重建组术中构建坐标系后,根据影像学模型关键孔定位规律定位关键孔圆心;对照组术中不构建坐标系,以星点为关键孔圆心定位关键孔,均常规行微血管减压术。术后 24 h 内构建影像学模型,测量骨窗面积、骨质缺损面积、术中实际关键孔圆心(R_0 点)与理想关键孔圆心(R 点)的距离(D值)。**结果** 基于影像科数据库内 80 例患者(160 侧)的影像学模型显示,以二腹肌沟顶点(A点)、颞鳞与顶乳缝交点(B点)和星点(C点)建立坐标系后, R 点坐标平均为 $[(4.60 \pm 3.89) \text{ mm}, (4.88 \pm 4.14) \text{ mm}]$,近似坐标点为 $(5 \text{ mm}, 5 \text{ mm})$;颞鳞与顶乳缝交点-二腹肌沟顶点连线与乙状窦沟上曲段重合率为 93.13%(149/160)、与乙状窦沟上曲段和垂直段重合率为 71.25%(114/160),颞鳞与顶乳缝交点-星点连线与横窦沟重合率为 95.63%(153/160)。基于 60 例手术患者手术前后影像学模型和术中所见显示,3 组患者骨窗面积、骨质缺损面积、D 值差异均具有统计学意义($P=0.000$),重建组和非重建组骨窗面积、骨质缺损面积和 D 值小于对照组(均 $P<0.01$),重建组骨窗面积($P=0.009$)和 D 值($P=0.000$)亦小于非重建组。**结论** 在不具备术前颅骨三维 CT 重建的条件下,以二腹肌沟顶点(A点)、颞鳞与顶乳缝交点(B点)和星点(C点)建立坐标系,以坐标点 $(5 \text{ mm}, 5 \text{ mm})$ 为关键孔圆心形成骨窗,可以较好定位关键孔。

【关键词】 颅骨; 解剖标志; 微血管减压术; 计算机,模拟; 神经解剖学

Localization of key holes in adult retrosigmoid sinus approach based on skull surface anatomic markers

FU Tao, HUI Zhi-qiang, SONG Jie, HUANG Jian, XU Peng

Department of Neurosurgery, Linyi Central Hospital, Linyi 276400, Shandong, China

Corresponding author: XU Peng (Email: 774529843@qq.com)

【Abstract】 Objective To explore the application value of skull surface markers which are easy to be exposed in the operation of retrosigmoid sinus approach to establish coordinate system in the location of key holes. **Methods** The thin slice CT of 80 patients with trigeminal neuralgia or hemifacial spasm from the image database of Linyi Central Hospital of Shandong Province from January 2019 to January 2020 were selected for three - dimensional (3D) imaging. The coordinate system was constructed by the vertex of digastric sulci (point A), the intersection of temporal scale and parietal lacustrine suture (point B) and star point (point C). A total of 60 patients who were hospitalized in our hospital from May 2020 to May 2022 and required retrosigmoid sinus approach for microvascular decompression (MVD) were selected and randomly divided into reconstruction group, non-reconstruction group and control group, with 20 cases in each group. In reconstruction group, after the construction of the coordinate system during the surgery, the

doi:10.3969/j.issn.1672-6731.2022.12.013

作者单位:276400 山东省临沂市中心医院神经外科

通讯作者:许鹏,Email:774529843@qq.com

center of key hole in 3D skull model constructed before surgery was used to locate the location. In non-reconstructed group, after the intraoperative construction of coordinate system, the key hole positioning law of the imaging model was used as the center of the key hole. In control group, no coordinate system was established during the operation, and the center of the key hole was taken as the star point. After the center of the key hole was determined, MVD was performed routinely in all groups. The 3D skull model was constructed after surgery, and bone window area, bone defect area, the actual center of key hole (R_0) and the center of ideal key hole (R, D value) were measured. **Results** The results of the imaging model showed the average coordinates of point R were $[(4.60 \pm 3.89) \text{ mm}, (4.88 \pm 4.14) \text{ mm}]$, and the approximate coordinates were (5 mm, 5 mm) after the establishment of the coordinate system with the vertex of digastric sulcus (point A), the intersection of temporal scale and parietal lacustrine suture (point B) and star point (point C). The coincidence rate between the intersection of temporal scale and parietal lacustrine suture and the transverse sinus groove was 95.63% (153/160), and the coincidence rate between the intersection of temporal scale and parietal lacustrine suture and the vertex of digastric sulcus and the superior curve of sigmoid sinus groove was 93.13% (149/160). The coincidence rate between the intersection of temporal scale and parietal lacustrine suture and the vertex line of digastric sulcus and the superior and vertical segment of sigmoid sulcus was 71.25% (114/160). The results showed the bone window area, bone defect area and D value were significantly different among 3 groups ($P = 0.000$, for all), and the bone window area, bone defect area and D value in reconstruction group and non-reconstruction group were all smaller than those in control group ($P < 0.01$, for all). Bone window area ($P = 0.009$) and D value ($P = 0.000$) in reconstructed group were also smaller than those in non-reconstructed group. **Conclusions** In the absence of preoperative CT 3D reconstruction of the skull, a coordinate system was established with the vertex of the digastric sulcus (point A), the intersection of temporal scale and parietal lacustrine suture (point B) and star point (point C), and a bone window was formed with the coordinate point (5 mm, 5 mm) as the center of the key hole to better locate the location of the key hole.

【Key words】 Skull; Anatomic landmarks; Microvascular decompression surgery; Computers, analog; Neuroanatomy

Conflicts of interest: none declared

乙状窦后入路是神经外科的常用手术入路,术中关键孔即横窦-乙状窦夹角(TSSJ)骨孔的准确定位是关键步骤,特别在面神经及三叉神经微血管减压术(MVD)等功能神经外科微创手术中具有重要意义^[1-3]。导静脉孔定位法、星点定位法、坐标系定位法等TSSJ定位方法可通过导静脉孔、星点、二腹肌沟顶点、颞鳞与顶乳缝交点、乳突尖、上项线等颅骨表面解剖标志进行定位^[4-8]。但临床实践中受手术切口的限制,乙状窦后入路手术中可直观显露的颅骨表面解剖标志较少,导致诸多TSSJ定位方法准确性较低^[5]。乙状窦后入路不仅需安全显露TSSJ,且要求最大程度减少术后骨质缺损面积,若术中骨质缺损面积较大,需行颅骨修补,会加重患者经济负担;若错误去除幕上骨质或损伤静脉窦,则加重手术创伤、增加手术风险。近年来,借助神经导航和增强现实(AR)技术的TSSJ定位方法虽可提高定位准确性,但因步骤复杂或成本较高,临床推广受限^[9-11]。鉴于此,本研究借助术中可显露的颅骨表面解剖标志构建坐标系,通过分析80例(160侧)影像学模型寻找关键孔定位规律,并选取60例患者进

行术中验证,以探寻更实用的TSSJ定位方法。

资料与方法

一、临床资料

1. 纳入标准 (1)三叉神经痛诊断为三叉神经分布区反复发作的阵发性剧烈疼痛,多呈单侧,偶见双侧先后发病,表现为撕裂样、电击样、针刺样、刀割样或烧灼样剧烈疼痛,可伴患侧流泪、流涎、流涕或面部抽搐,存在触发点或扳机点,通常位于上下唇、鼻翼、鼻唇沟、牙龈、颊部、口角等,可因咀嚼、进食、饮水、风吹、寒冷、刷牙、洗脸、说话等动作诱发^[12]。(2)面肌痉挛诊断为存在单侧或双侧面部肌肉(眼轮匝肌、表情肌、口轮匝肌)反复发作的阵发性、不自主抽搐,情绪激动或紧张时加重,严重者可出现睁眼困难、口角歪斜和耳内抽动感杂音,且术中电生理监测存在异常肌反应^[12]。(3)舌咽神经痛诊断为发作性疼痛局限于单侧舌根、扁桃体区、咽部、下颌角、乳突区、外耳道区等,可因吞咽、咀嚼、说话、咳嗽、哈欠等动作诱发^[12]。(4)均为首次行乙状窦后入路微血管减压术。(5)年龄 > 18 岁。(6)本

表 1 不同处理组患者一般资料的比较
Table 1. Comparison of clinical data among different treatment groups

| 观察指标 | 对照组 (n=20) | 非重建组 (n=20) | 重建组 (n=20) | 统计 量值 | P 值 |
|---|----------------------|----------------------|----------------------|----------|-------------|
| 性别[例(%)] | | | | | 0.950 0.622 |
| 男性 | 10(50.00) | 9(45.00) | 7(35.00) | | |
| 女性 | 10(50.00) | 11(55.00) | 13(65.00) | | |
| 年龄($\bar{x} \pm s$, 岁) | 57.80 ± 10.42 | 61.40 ± 12.05 | 59.35 ± 12.47 | 0.478 | 0.623 |
| 病程 [M(P ₂₅ , P ₇₅), 年] | 2.42 (1.00, 4.00) | 1.96 (0.84, 2.88) | 2.00 (1.17, 3.13) | 1.501 | 0.472 |
| 受教育程度 [M(P ₂₅ , P ₇₅), 年] | 5.75 (1.25, 9.00) | 6.35 (1.25, 9.00) | 6.85 (5.00, 9.00) | 0.523 | 0.770 |
| 高血压[例(%)] | 6(30.00) | 7(35.00) | 8(40.00) | 0.440 | 0.803 |
| 冠心病[例(%)] | 6(30.00) | 5(25.00) | 6(30.00) | 0.164 | 0.921 |
| 糖尿病[例(%)] | 4(20.00) | 6(30.00) | 7(35.00) | 1.149 | 0.563 |
| 高脂血症[例(%)] | 6(30.00) | 9(45.00) | 5(25.00) | 1.950 | 0.377 |
| 吸烟[例(%)] | 7(35.00) | 5(25.00) | 4(20.00) | 1.193 | 0.551 |
| 饮酒[例(%)] | 6(30.00) | 8(40.00) | 5(25.00) | 1.078 | 0.583 |
| 三叉神经痛[例(%)] | 11(50.00) | 10(50.00) | 12(60.00) | 0.404 | 0.817 |
| 面肌痉挛[例(%)] | 9(45.00) | 9(45.00) | 7(35.00) | 0.549 | 0.760 |
| 舌咽神经痛[例(%)] | 0(0.00) | 1(5.00) | 1(5.00) | 1.276 | 1.000 |

One-way ANOVA test for comparison of age, Kruskal-Wallis test (H test) for comparison of duration and education, Fisher's exact probability for comparison of glossopharyngeal neuralgia, and χ^2 test for comparison of others, 年龄的比较行单因素方差分析, 病程和受教育程度的比较行 Kruskal-Wallis 检验(H 检验), 舌咽神经痛的比较行 Fisher 确切概率法, 其余指标的比较行 χ^2 检验

研究经山东省临沂市中心医院道德伦理委员会审核批准(审批号: LYSZXY2020030)。(7)均于术前向患者及其家属告知手术方式和手术风险并签署知情同意书。

2. 排除标准 (1)其他疾病需行乙状窦后入路微血管减压术。(2)颅骨病变或发育畸形。

3. 一般资料 选择 2020 年 5 月至 2022 年 5 月在山东省临沂市中心医院神经外科行乙状窦后入路微血管减压术的患者共 60 例, 临床诊断为三叉神经痛 33 例(55%), 面肌痉挛 25 例(41.67%), 舌咽神经痛 2 例(3.33%)。男性 26 例, 女性 34 例; 年龄为 25 ~ 82 岁, 平均(59.52 ± 11.58)岁; 受教育程度 0 ~ 16 年, 中位值 5(5, 9)年; 病程 0.50 ~ 5.75 年, 中位病程为 2.00(1.00, 3.50)年; 既往有高血压 21 例(35%)、冠心病 17 例(28.33%)、糖尿病 17 例(28.33%)、高脂血症 20 例(33.33%), 吸烟 16 例(26.67%)、饮酒 19 例(31.67%)。根据定位关键孔的方法, 采用随机数字表法随机分为重建组、非重建组和对照组, 每组各 20 例。3 组患者一般资料比较, 差异无统计学意义

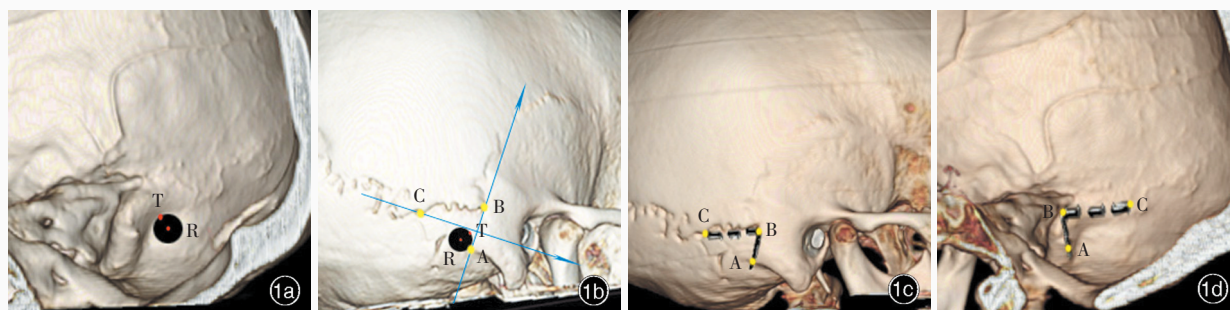
(均 $P > 0.05$, 表 1), 均衡可比。

二、研究方法

1. 影像学模型构建 选取我院影像科数据库 2019 年 1 月至 2020 年 1 月共 80 例患者(包括三叉神经痛 44 例、面肌痉挛 36 例)计 160 侧颅骨薄层(层厚 1 mm)CT 数据。将原始图像导入 E-3D(V17.08)软件(<http://www.e3d-med.com/download>)进行三维成像及参数测量。参照文献[7]方法构建模型, 采用软件自带的“剪切工具”对重建的三维颅骨模型进行剪切, 观察目标区域颅骨内外侧解剖结构, 标记关键孔与 TSSJ 内侧缘的切点为 T 点, 采用“圆形剪切工具”在 TSSJ 内侧缘剪切出直径 1 cm 的模拟关键孔并标记圆心为 R 点(图 1a); 调整颅底外侧面方向, 使之与术中术者视角一致, 确保钻孔方向与颅骨表面垂直; 再将 3D CT 图像翻转 180°, 显示颅底内侧面和 TSSJ。参照《RHOTON 颅脑解剖与手术入路》^[13]识别并标记颅骨表面解剖标志, 以二腹肌后腹附着骨质凹陷形成的二腹肌沟最高点为二腹肌沟顶点(A 点), 以颞骨鳞部与顶骨之间骨缝与顶乳缝的交点为颞鳞与顶乳缝交点(B 点), 以人字缝、顶乳缝、枕乳缝交点为星点(C 点), 连接 A 点与 B 点作 y 轴, 经 C 点做 y 轴垂线为 x 轴, 采用“测量工具”测量 T 点和 R 点在坐标系中的位置及其与 C 点的距离(图 1b); 采用“矩形剪切工具”在三维颅骨模型上标记线段 AB 和线段 BC, 观察二者与横窦沟和乙状窦沟的位置关系(图 1c, 1d), 若线段 AB 与乙状窦沟上曲段重合则认为其可作为乙状窦沟上曲段的表面标志, 若线段 AB 同时与乙状窦沟上曲段和垂直段重合则认为其可作为乙状窦沟上曲段和垂直段的表面标志, 若线段 BC 与横窦沟重合则认为其可作为横窦沟的表面标志, 并计算线段 AB 和线段 BC 与横窦沟和乙状窦沟的重合率, 公式为重合率(%) = 重合例数 / 总例数 × 100%。

2. 术前影像学检查 所有手术患者术前均行颅骨薄层 CT 扫描, 同法构建术前影像学模型坐标系, 重建组和非重建组标记关键孔圆心(R 点)、对照组标记星点(C 点)为理想关键孔圆心, 并计算坐标值。

3. 手术方法 (1)术中定位关键孔: ①重建组, 根据术前影像学模型于颅骨外侧面定位关键孔圆心(R 点)。患者侧卧位, 病灶侧朝上, 全身麻醉下取耳后直切口, 长度 5 ~ 6 cm, 逐层切开头皮、皮下组织及肌肉, 乳突牵开器撑开切口, 剥离骨膜, 显露颅骨, 确认 A 点、B 点和 C 点位置, 过氧化氢溶液和生



T点, 关键孔与TSSJ内侧缘的切点; R点, 关键孔圆心; A点, 二腹肌沟顶点; B点, 颞鳞与顶乳缝交点; C点, 星点

图1 3D颅骨重建模型参数测量 1a 标记关键孔与TSSJ内侧缘的切点为T点,通过“圆形剪切工具”在TSSJ内侧缘形成模拟关键孔,标记圆心R点 1b 将模型翻转180°后标记A点、B点和C点,连接A点与B点,经C点做线段AB垂线并构建坐标系,T点坐标为(1.30 mm, 3.40 mm)、R点坐标为(5 mm, 5 mm),T点与星点相距22.50 mm、R点与星点相距19.60 mm 1c 标记线段AB和线段BC 1d 将模型翻转180°后可见线段AB与乙状窦沟上曲段和垂直段重合,线段BC与横窦沟重合

Figure 1 Parameters measurement of skull 3D reconstruction model Marking the apex of the inner edge of TSSJ as point T, using the circular shear tool to form virtual key hole on the inner edge of TSSJ, and marking the center of the circle point R (Panel 1a). Marking point A, point B and point C after rotating the model of 180°. Connecting point A and point B, making a vertical line of AB through point C, extending the 2 lines to build the coordinate system, the coordinate of point T was (1.30 mm, 3.40 mm), the coordinate of point R was (5 mm, 5 mm), the distance between point T and asterion was 22.50 mm, the distance between point R and asterion was 19.60 mm (Panel 1b). Marking line segment AB and BC (Panel 1c). The AB was observed to coincide with the superior curved and vertical segments of sigmoid sulcus, and the BC coincided with the transverse sinus sulcus after the model was rotated 180° (Panel 1d).

理盐水交替冲洗术区,使人字缝、顶乳缝、枕乳缝、颞鳞等结构清晰可辨,以无菌尖镊蘸取亚甲蓝连接A点和B点,经C点做线段AB垂线,建立坐标系,据术前影像学模型模拟的关键孔坐标值定位关键孔圆心(图2)。(2)非重建组,术前行CT检查但不构建影像学模型。采用与重建组同样的方法于术中建立坐标系,以坐标点(5 mm, 5 mm)为关键孔圆心,仅1例因模拟关键孔范围跨过颞鳞与顶乳缝交点-星点连线3 mm,将钻孔位置下移3 mm,在确保不跨越颞鳞与顶乳缝交点-二腹肌沟顶点连线的前提下建立关键孔。(3)对照组,术前不构建影像学模型、术中不建立坐标系,仅以星点(C点)为关键孔圆心。(2)形成骨窗:3组患者准确定位关键孔后,以直径1 cm钻头钻出关键孔,铣刀形成直径为2.50 cm的骨窗,如果横窦和乙状窦显露不充分,则以咬骨钳去除骨质,扩大骨窗至充分显露。(3)常规行微血管减压术。

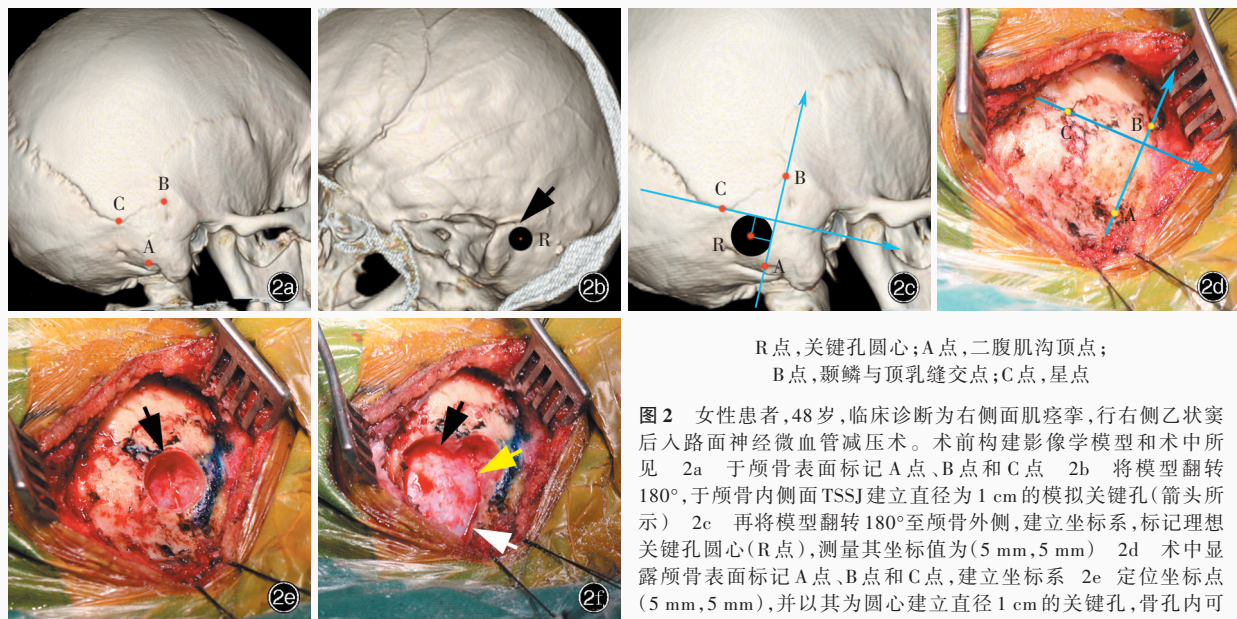
4. 术后影像学指标评估 术后24 h内复查颅骨薄层CT并将数据导入E-3D(V17.08)软件进行三维成像。(1)骨窗面积及骨质缺损面积测量:采用软件自带的“多边形测量工具”测量术后骨瓣面积(S_1)和骨窗面积(S_2),二者差值($S_2 - S_1$)即为术后骨质缺损面积(S_0)。(2)实际关键孔圆心与理想关键孔圆心距离测量:同法构建术后影像学模型,重建组和非重建组将关键孔残缘在术后影像学模型上复原为直

径1 cm的关键孔,标记圆心即为实际关键孔圆心(R_0 点),对照组星点(C点)即为 R_0 点;再根据术前影像学模型的理想关键孔圆心(R点)坐标在术后影像学模型上标记R点,并采用“测量工具”测量 R_0 点与R点的距离(D值)。

5. 统计分析方法 采用SPSS 17.0统计软件进行数据处理与分析。计数资料以相对数构成比(%)或率(%)表示,采用 χ^2 检验或Fisher确切概率法。正态性检验采用Shapiro-Wilk检验,呈正态分布的计量资料以均数 \pm 标准差($\bar{x} \pm s$)表示,采用单因素方差分析,两两比较行LSD- t 检验;呈非正态分布的计量资料以中位数和四分位数间距[$M(P_{25}, P_{75})$]表示,采用Kruskal-Wallis检验(H 检验)。以 $P \leq 0.05$ 为差异具有统计学差异。

结 果

基于影像科数据库内80例患者(160侧)的影像学模型显示,T点坐标平均为[(0.27 \pm 3.50) mm, (2.26 \pm 4.03) mm],T点与星点平均距离为(18.19 \pm 5.13) mm;R点的坐标平均为[(4.60 \pm 3.89) mm, (4.88 \pm 4.14) mm],R点与星点平均距离为(16.59 \pm 4.34) mm;颞鳞与顶乳缝交点-二腹肌沟顶点连线(线段AB)与乙状窦沟上曲段重合率为93.13%(149/160),颞鳞与顶乳缝交点-二腹肌沟顶点连线(线段AB)与乙状窦沟上曲段和垂直段重合率为71.25%



R点,关键孔圆心;A点,二腹肌沟顶点;
B点,颞鳞与顶乳缝交点;C点,星点

图2 女性患者,48岁,临床诊断为右侧面肌痉挛,行右侧乙状窦后入路面神经微血管减压术。术前构建影像学模型和术中所见 2a 于颅骨表面标记A点、B点和C点 2b 将模型翻转180°,于颅骨内侧面TSSJ建立直径为1cm的模拟关键孔(箭头所示) 2c 再将模型翻转180°至颅骨外侧,建立坐标系,标记理想关键孔圆心(R点),测量其坐标值为(5mm,5mm) 2d 术中显露颅骨表面标记A点、B点和C点,建立坐标系 2e 定位坐标点(5mm,5mm),并以其为圆心建立直径1cm的关键孔,骨孔内可见TSSJ(箭头所示) 2f 制备骨窗,骨窗大小为5.07cm²,其内可

见TSSJ(黄色箭头所示)、横窦边缘(黑色箭头所示)、乙状窦边缘(白色箭头所示)

Figure 2 A 48-year-old female was diagnosed with right hemifacial spasm, right retrosigmoid sinus approach microvascular decompression of facial nerve was performed. Preoperative construction of imaging model and surgical findings A 3D skull model was established to identify 3 points of point A, point B and point C (Panel 2a). Rotating the model with 180°, a simulated key hole with a diameter of 1 cm was established at the TSSJ on the inner side of the skull (arrow indicates, Panel 2b). Rotating the model with 180° to the outside of the skull, establishing the rectangular coordinate system. The virtual key hole center point R was marked, its coordinate value was measured as (5 mm, 5 mm; Panel 2c). Three points A, B and C were exposed during the surgery to establish the coordinate system (Panel 2d). The coordinate point (5 mm, 5 mm) was found, and establishing the key hole with 1 cm of diameter (arrow indicates). The transverse-sigmoid sinus junction could be seen in the bone hole (Panel 2e). The transverse-sigmoid sinus junction (yellow arrow indicates), transverse sinus margin (black arrow indicates), and sigmoid sinus margin (white arrow indicates) could be observed in the bone window, while the bone window area was 5.07 cm² (Panel 2f).

(114/160),颞鳞与顶乳缝交点-星点连线(线段BC)与横窦沟的重合率为95.63%(153/160)。

基于60例手术患者的手术前后影像学模型及术中所见,重建组有15例关键孔位于TSSJ,3例关键孔仅显露乙状窦,距横窦下缘平均距离为(2.54 ± 0.87) mm,2例关键孔仅显露横窦,距乙状窦上曲段平均距离为(2.05 ± 0.68) mm;非重建组有13例关键孔位于TSSJ,7例关键孔仅显露乙状窦,距横窦下缘平均距离为(3.98 ± 1.49) mm。重建组和非重建组无一例术中需钛网修补颅骨缺损;对照组有3例因骨瓣过小无法还纳,术中使用钛网修补颅骨缺损。

3组患者骨窗面积、骨质缺损面积和D值差异均具有统计学意义($P=0.000$,表2),其中,重建组和非重建组骨窗面积、骨质缺损面积和D值小于对照组(均 $P<0.01$),重建组骨窗面积($P=0.009$)和D值($P=0.000$)亦小于非重建组(表3)。

讨 论

乙状窦后入路主要应用于脑桥小脑角肿瘤、三

叉神经痛、面神经痉挛等疾病的手术治疗^[1]。乙状窦后入路可充分显露脑神经(第IV~XI对)、椎基底动脉、脑干等解剖结构,这些结构解剖关系复杂,手术过程中稍有不慎即可导致听力损失、面瘫、饮水呛咳等并发症;若损伤椎动脉(VA)和基底动脉(BA)等脑干供血动脉或脑干组织,则严重危害患者生命健康^[14-15]。TSSJ的准确定位一直被认为是乙状窦后入路手术中的关键步骤,此处钻孔形成的骨窗可以较好显露横窦和乙状窦边缘,最大程度显露硬膜下结构,减少脑组织牵拉。

TSSJ解剖变异较大,星点和导静脉孔是常用的定位标志。导静脉孔定位法以乳突后方上项线以下最大的导静脉孔为关键孔圆心进行TSSJ定位^[5],但可能出现导静脉孔缺如的情况,Louis等^[16]通过对100例尸头标本和100例颅骨标本观察发现,4例(2%)标本右侧无导静脉孔,56例(28%)标本左侧无导静脉孔。星点定位法以星点为关键孔圆心进行TSSJ定位^[5],Muche^[17]共收集61例埃塞俄比亚西北部成人颅骨标本,采用游标卡尺测量星点至TSSJ距

表 2 不同处理组骨窗面积、骨质缺损面积和 D 值的比较 ($\bar{x} \pm s$)

Table 2. Comparison of bone window area, bone defect area and D value among different treatment groups ($\bar{x} \pm s$)

| 组别 | 例数 | 骨窗面积(cm ²) | 骨质缺损面积(cm ²) | D 值(mm) |
|---------|----|------------------------|--------------------------|--------------|
| 对照组(1) | 20 | 7.92 ± 1.53 | 4.49 ± 1.16 | 15.47 ± 4.63 |
| 非重建组(2) | 20 | 6.88 ± 0.45 | 1.95 ± 0.31 | 7.75 ± 3.97 |
| 重建组(3) | 20 | 6.00 ± 0.77 | 1.64 ± 0.16 | 1.73 ± 0.63 |
| F 值 | | 17.696 | 99.696 | 75.670 |
| P 值 | | 0.000 | 0.000 | 0.000 |

表 3 不同处理组骨窗面积、骨质缺损面积和 D 值的两两比较

Table 3. Pairwise comparison of bone window area, bone defect area and D value among different treatment groups

| 组间两两比 | 骨窗面积 | | 骨质缺损面积 | | D 值 | |
|---------|--------|-------|---------|-------|---------|-------|
| | t 值 | P 值 | t 值 | P 值 | t 值 | P 值 |
| (1):(2) | -3.240 | 0.002 | -11.473 | 0.000 | -6.892 | 0.000 |
| (1):(3) | -5.941 | 0.000 | -12.866 | 0.000 | -12.271 | 0.000 |
| (2):(3) | 2.701 | 0.009 | 1.393 | 0.169 | 5.379 | 0.000 |

离, 37 例(60.66%) TSSJ 位于星点, 24 例(39.34%) TSSJ 高于星点, 因此认为星点无法代表 TSSJ。为提高 TSSJ 定位准确性, 研究者不断尝试对其定位方式进行量化。Teranishi 等^[18]以横窦上缘切线为 x 轴, 以乙状窦外侧缘切线为 y 轴构建坐标系, 并以星点前方(x 轴方向)6.5 mm、下方(y 轴方向)6.5 mm 处为关键孔圆心; Ribas 等^[19]将星点前方(顶乳缝方向)10 mm、顶乳缝垂直下方 5 mm 处作为关键孔圆心; Tubbs 等^[8]以颞弓上缘的延长线为 x 轴, 以经过二腹肌沟顶点的颞弓上缘垂线为 y 轴, 构建坐标系, 关键孔圆心坐标为(10 mm, 5 mm); Li^[6]等以颞弓上缘延长线为 x 轴, 经乳突尖做 x 轴垂线为 y 轴, 关键孔圆心坐标为(23 mm, 3.5 mm); Hall 等^[5]收集 50 例新西兰人颅骨薄层 CT 数据, 建立 3D 颅骨模型, 并对上述定位方法进行对比分析, 发现导静脉孔法、星点法, 以及 Teranishi 等^[18]、Ribas 等^[19]、Li 等^[6]、Tubbs 等^[8]方法定位的实际关键孔圆心与理想关键孔圆心的距离(D 值)平均为 12.04、13.85、7.77、6.62、6.30 和 6.83 mm; 与前两种方法相比, 后 4 种方法定位 TSSJ 的准确性更高, 但该项研究仅通过 3D CT 颅骨重建模型进行对比, 未进行手术验证。临床实践中, Teranishi 等^[18]的定位方法将横窦上缘切线(x 轴)及乙状窦外侧缘切线(y 轴)设为假想线, 实际上术中难以定位坐标系且顶乳缝难以近似看作一条直线,

导致误差; Ribas 等^[19]的定位方法也存在相同问题; Li 等^[6]和 Tubbs 等^[8]的定位方法虽然较导静脉孔法和星点法的定位准确性更高, 但依赖颞弓和乳突尖等手术显露区域以外的颅骨表面标志辅助定位, 易因术中皮肤和肌肉等软组织覆盖、无菌手术巾遮挡等因素影响定位准确性。Xia 等^[7]根据术中可显露的颅骨标志二腹肌沟顶点及星点构建坐标系, 以二腹肌沟顶点与星点的连线为 x 轴, 以过星点的 x 轴垂线为 y 轴, 结合术前 3D CT 定位 TSSJ, 可显著提高定位准确性, 且避免静脉窦损伤的风险。

Day 等^[20]对 15 例尸头标本进行测量, 发现颞鳞与顶乳缝交点位于乙状窦上曲段外侧缘, 故颞鳞和顶乳缝交点与乳突尖的连线可以作为乙状窦全长的投影, 为术中保护乙状窦提供可靠依据。随着乙状窦后入路开颅手术逐渐趋向微创化, 术中较少显露乳突尖, 给术中定位乙状窦带来困难。受手术切口的限制, 颞鳞与顶乳缝交点是乙状窦后入路手术中除星点、二腹肌沟顶点外最常显露的颅骨表面解剖标志, 故本研究将颞鳞与顶乳缝交点作为 TSSJ 定位的参考点, 结果显示, 颞鳞与顶乳缝交点-星点连线和颞鳞与顶乳缝交点-二腹肌沟顶点连线与横窦沟和乙状窦沟上曲段的重合率分别为 95.63%(153/160)和 93.13%(149/160), 可较好反映横窦沟和乙状窦沟上曲段的解剖位置。本研究非重建组术中根据二腹肌沟顶点、颞鳞与顶乳缝交点、星点构建坐标系, 以影像学模型模拟的关键孔圆心[(4.60 ± 3.89) mm, (4.88 ± 4.14) mm]的近似坐标点(5 mm, 5 mm)为关键孔圆心进行钻孔, 成功定位 TSSJ 的概率为 60%(12/20); 重建组亦存在实际关键孔圆心与理想关键孔圆心不一致的现象, 这可能与大部分患者在该区域存在乳突上嵴, 导致术中钻孔区域骨面不平整, 使颅骨钻孔方向无法垂直于骨面有关。

不同外科手术中乙状窦后入路对骨窗的要求不尽相同, 三叉神经微血管减压术要求骨窗可良好显露横窦、乙状窦边缘^[21]; 面神经及舌咽神经微血管减压术对骨窗的要求稍低, 主要显露乙状窦边缘即可^[22]。本研究非重建组术中乙状窦显露率为 95%(19/20), 且无一例使用钛网修补骨窗。Dao Trong 等^[23]从人脑连接组学计划(Human Connectome Project)中筛选 60 例亚洲人、57 例非洲裔美国人和 70 例白种人的横断面、冠状位及矢状位头部薄层 T₂WI 图像, 采用 3D Slicer 软件进行重建, 并测量 TSSJ 与内听道的相对距离, 发现不同种族之

间 TSSJ 定位存在差异,非洲裔美国人 TSSJ 位置最高,然后依次为亚洲人和白种人。

本研究仅纳入部分国内人群,样本量较小,且构建影像学模型探寻 TSSJ 定位规律时未纳入舌咽神经痛病例,存在研究对象选择偏倚,未来尚待扩大样本量、纳入更多疾病类型进一步验证本研究结果的适用性。

综上所述,以乙状窦后入路手术较易显露的二腹肌沟顶点(A点)、颞鳞与顶乳缝交点(B点)和星点(C点)为参考点,术中根据上述3个可视的颅骨表面解剖标志建立坐标系,以坐标点(5 mm, 5 mm)为关键孔圆心形成骨窗,可较好定位 TSSJ,且无骨瓣缺损,为无法进行术前颅骨三维 CT 重建的患者提供便利。

利益冲突 无

参 考 文 献

- [1] Basma J, Anagnostopoulos C, Tudose A, Harty M, Michael LM 2nd, Teo M, Porter DG. History, variations, and extensions of the retrosigmoid approach: anatomical and literature review[J]. *J Neurol Surg B Skull Base*, 2021, 83(Suppl 2):e324-335.
- [2] Chen S, Yang N, Li W, Xu S, Li X, Ma X. A standard operation procedure of clean and fast craniotomy technique for retrosigmoid approach[J]. *J Craniofac Surg*, 2019, 30: 1774-1776.
- [3] Ricci G, Di Stadio A, D'Ascanio L, La Penna R, Trabalzini F, Della Volpe A, Magnan J. Endoscope - assisted retrosigmoid approach in hemifacial spasm: our experience [J]. *Braz J Otorhinolaryngol*, 2019, 85:465-472.
- [4] Li R, Qi L, Yu X, Li K, Bao G. Mastoid notch as a landmark for localization of the transverse - sigmoid sinus junction [J]. *BMC Neurol*, 2020, 20:111.
- [5] Hall S, Peter Gan YC. Anatomical localization of the transverse-sigmoid sinus junction: comparison of existing techniques [J]. *Surg Neurol Int*, 2019, 10:186.
- [6] Li RC, Liu JF, Li K, Qi L, Yan SY, Wang MD, Xie WF. Localization of anterosuperior point of transverse-sigmoid sinus junction using a reference coordinate system on lateral skull surface [J]. *Chin Med J (Engl)*, 2016, 129:1845-1849.
- [7] Xia L, Zhang M, Qu Y, Ren M, Wang H, Zhang H, Yu C, Zhu M, Li J. Localization of transverse-sigmoid sinus junction using preoperative 3D computed tomography: application in retrosigmoid craniotomy [J]. *Neurosurg Rev*, 2012, 35:593-598.
- [8] Tubbs RS, Loukas M, Shoja MM, Bellew MP, Cohen-Gadol AA. Surface landmarks for the junction between the transverse and sigmoid sinuses: application of the "strategic" burr hole for suboccipital craniotomy [J]. *Neurosurgery*, 2009, 65(6 Suppl):37-41.
- [9] da Silva EB Jr, Leal AG, Milano JB, Da Silva LF Jr, Clemente RS, Ramina R. Image - guided surgical planning using anatomical landmarks in the retrosigmoid approach [J]. *Acta Neurochir (Wien)*, 2010, 152:905-910.
- [10] Jiang S, Huo XH, Sun MR, Hou Q, Liu MT, Tian JH. Application of augmented reality assisted three dimensional CT in retrosigmoid craniotomy [J]. *Zhonghua Shen Jing Wai Ke Za Zhi*, 2018, 34:619-622. [蒋帅, 霍显浩, 孙美蓉, 侯乾, 刘茂唐, 田继辉. 增强现实技术辅助 CT 三维重建在经乙状窦后入路开颅手术中的应用 [J]. *中华神经外科杂志*, 2018, 34:619-622.]
- [11] Legninda Sop FY, D'Ercole M, Izzo A, Rapisarda A, Ioannoni E, Caricato A, Olivi A, Montano N. The impact of neuronavigation on the surgical outcome of microvascular decompression for trigeminal neuralgia [J]. *World Neurosurg*, 2021, 149:80-85.
- [12] Zhou LF. *Modern neurosurgery* [M]. 2th ed. Shanghai: Fudan University Press, 2015: 1257-1278. [周良辅. 现代神经外科学 [M]. 2版. 上海: 复旦大学出版社, 2015: 1257-1278.]
- [13] Rhoton AL. *Rhoton's cranial anatomy and surgical approaches* [M]. Liu QL, Trans. Beijing: China Science and Technology Press, 2010: 643-699. [Rhoton AL. RHOTON 颅脑解剖与手术入路 [M]. 刘庆良, 译. 北京: 中国科学技术出版社, 2010: 643-699.]
- [14] Cheng Y, Song Y, Wei Y, Geng H, Wu X, Li M, Liang J, Song G. Safe region of craniotomy to access the cerebellopontine region by retrosigmoid approach: a radiological and anatomical study [J]. *J Craniofac Surg*, 2022. [Epub ahead of print]
- [15] González - Darder JM, Capilla - Guasch P, Real - Peña L. Retrosigmoid approach: a simple and safe way to resect intrinsic pontomedullary lesions [J]. *J Neurol Surg B Skull Base*, 2020, 81:223-231.
- [16] Louis RG Jr, Loukas M, Wartmann CT, Tubbs RS, Apaydin N, Gupta AA, Spentzouris G, Ysique JR. Clinical anatomy of the mastoid and occipital emissary veins in a large series [J]. *Surg Radiol Anat*, 2009, 31:139-144.
- [17] Mucche A. Morphometry of asterion and its proximity to dural venous sinuses in northwest ethiopian adult skulls [J]. *J Craniofac Surg*, 2021, 32:1171-1173.
- [18] Teranishi Y, Kohno M, Sora S, Sato H. Determination of the keyhole position in a lateral suboccipital retrosigmoid approach [J]. *Neurol Med Chir (Tokyo)*, 2014, 54:261-266.
- [19] Ribas GC, Rhoton AL Jr, Cruz OR, Peace D. Suboccipital burr holes and craniectomies [J]. *Neurosurg Focus*, 2005, 19:E1.
- [20] Day JD, Kellogg JX, Tschabitscher M, Fukushima T. Surface and superficial surgical anatomy of the posterolateral cranial base: significance for surgical planning and approach [J]. *Neurosurgery*, 1996, 38:1079-1083.
- [21] Agarwal N, Kumar A, Singh P, Chandra PS, Kale SS. Suprameatal extension of retrosigmoid approach in microvascular decompression for trigeminal neuralgia with petrous endostosis: case report and literature review [J]. *Neurol India*, 2022, 70:1240-1243.
- [22] Guo X, Zhang C, Li Y, Li X, Ma X, Li W. Fully endoscopic microvascular decompression for hemifacial spasm using improved retrosigmoid infraorbital approach: clinical analysis of 81 cases [J]. *Oper Neurosurg (Hagerstown)*, 2022, 23:40-45.
- [23] Dao Trong P, Beynon C, Unterberg A, Schneider T, Jesser J. Racial differences in the anatomy of the posterior fossa: neurosurgical considerations [J]. *World Neurosurg*, 2018, 117: e571-e574.

(收稿日期:2022-12-16)

(本文编辑:柏钰)